Green and Sustainable Chemistry, 2017, 7, 57-69
http://www.scirp.org/journal/gsc
ISSN Online: 2160-696X
ISSN Print: 2160-6951

Optical Analysis of a ZnO/Cu_2O Subcell in a Silicon-Based Tandem Heterojunction Solar Cell

Ørnulf Nordseth[1], Raj Kumar[2], Kristin Bergum[2], Laurenţiu Fara[3,4], Sean Erik Foss[1], Halvard Haug[1], Florin Drăgan[3*], Dan Crăciunescu[3], Paul Sterian[3,4], Irinela Chilibon[5], Cristina Vasiliu[5], Laurentiu Baschir[5], Dan Savastru[5], Edouard Monakhov[2], Bengt Gunnar Svensson[2]

[1]Institute for Energy Technology (IFE), Kjeller, Norway
[2]Department of Physics/Center for Materials Science and Nanotechnology (SMN), University of Oslo, Oslo, Norway
[3]University Politehnica of Bucharest, Bucharest, Romania
[4]Academy of Romanian Scientists, Bucharest, Romania
[5]National Institute of Research and Development for Optoelectronics (INOE-2000), Bucharest, Romania
Email: *florin.dragan@sdettib.pub.ro

How to cite this paper: Nordseth, Ø., Kumar, R., Bergum, K., Fara, L., Foss, S.E., Haug, H., Drăgan, F., Crăciunescu, D., Sterian, P., Chilibon, I., Vasiliu, C., Baschir, L., Savastru, D., Monakhov, E. and Svensson, B.G. (2017) Optical Analysis of a ZnO/Cu_2O Subcell in a Silicon-Based Tandem Heterojunction Solar Cell. *Green and Sustainable Chemistry*, **7**, 57-69.
https://doi.org/10.4236/gsc.2017.71005

Received: January 25, 2017
Accepted: February 24, 2017
Published: February 27, 2017

Abstract

Research on silicon-based tandem heterojunction solar cells (STHSC) incorporating metal oxides is one of the main directions for development of high-efficiency solar cells. In this work, the optical characteristics of a STHSC consisting of a ZnO/Cu_2O subcell on top of a silicon-based subcell were studied by optical modelling. Cu_2O is a direct-gap p-type semiconductor which is attractive for application in solar cells due to its high absorptance of ultra-violet and visible light, nontoxicity, and low-cost producibility. Highly Al-doped ZnO and undoped Cu_2O thin films were prepared on quartz substrates by magnetron sputter deposition. Thermal annealing of the Cu_2O layer at 900˚C enhances the electrical properties and reduces optical absorption, presumably as a result of increased grain size. Hall effect measurements show that the majority carrier (hole) mobility increases from 10 to 50 $cm^2/V{\cdot}s$ and the resistivity decreases from 560 to 200 Ω·cm after annealing. A Cu_2O absorber layer of 2 μm thickness will generate about 10 mA/cm^2 of photocurrent under AM1.5G illumination. The optical analysis of the STHSC involved calculating the spectral curves for absorptance, transmittance, and reflectance for different thicknesses of the thin film layers constituting the ZnO/Cu_2O subcell. The complex refractive indices of the thin films were derived from spectroscopic ellipsometry measurements and implemented in the simulation model. The lowest reflectance and highest transmittance for the ZnO/Cu_2O subcell are obtained for a thickness of approximately 80 nm for both the top

and bottom AZO layers. The SiN_x anti-reflection coating for the c-Si bottom subcell must be optimized to accommodate the shift of the photon spectrum towards longer wavelengths. By increasing the thickness of the SiN_x layer from 80 nm to 120 nm, the total reflectance for the STHSC device is reduced from 12.7% to 9.7%.

Keywords

Tandem Solar Cells, Heterojunction, Cuprous Oxide, Magnetron Sputtering, Optical Properties, Optical Modelling

1. Introduction

Rapid progress of thin film solar cells has resulted in the development of tandem solar cells based on crystalline silicon with conversion efficiencies beyond the c-Si single-junction limit [1] [2] [3]. Such cell concepts are needed to ensure competitiveness of solar power with conventional energy sources. In recent years, tandem solar cells have been successfully implemented for various technologies, including solar cells based on III-V type semiconductors and monocrystalline, polycrystalline, and amorphous silicon, dye sensitized solar cells, and quantum dot solar cells [3] [4] [5] [6]. However, the manufacturing of silicon-based tandem heterojunction solar cells (STHSC) with a high efficiency at low cost has still not been accomplished. This situation might soon be changed due to the swift development of perovskite thin films as photovoltaic absorbents, showing a remarkable progress in the last 5 years [7] [8]. Another promising material for implementation in STHSC is cuprous oxide (Cu_2O). This semiconducting metal oxide has a high optical absorption, is non-toxic, and has the potential for low production cost [9] [10]. The theoretical limit of the conversion efficiency for a solar cell based on Cu_2O is approximately 20% under one sun illumination [11]. However, the highest conversion efficiency achieved experimentally is 8.1% for a ZnO/Cu_2O solar cell based on thermally oxidized copper sheets [12], suggesting that further investigation of Cu_2O-based solar cells is still needed in order to realize their full potential in photovoltaic applications.

The objective of this work is to evaluate the optical performance of a ZnO/Cu_2O subcell in a Si-based tandem heterojunction solar cell (STHSC) configuration. **Figure 1** shows a schematic device design of a STHSC, combining a conventional crystalline silicon subcell with a ZnO/Cu_2O subcell in a mechanical stack of independently connected cells, *i.e.* a four-terminal configuration. The relatively high band gap of Cu_2O (E_g = 2.1 eV), which is approximately 1 eV higher than that of crystalline silicon (E_g = 1.13 eV), makes it challenging to realize a low-cost monolithic (two-terminal) tandem configuration. In general, a four-terminal configuration allows accessing a wider range of material combinations compared to a two-terminal configuration since there is less constraint on current matching for the two subcells.

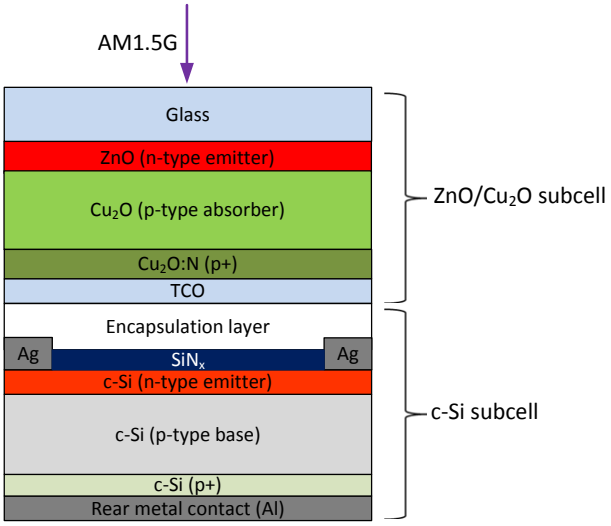

Figure 1. Schematic device design of a four-terminal tandem heterojunction solar cell combining a conventional crystalline silicon bottom subcell with a metal oxide top subcell based on ZnO and Cu_2O layers.

The ZnO/Cu_2O subcell is realized by reactive magnetron sputter deposition of metal oxides on a transparent glass substrate (quartz), enabling low-energy photons to be transmitted through the ZnO/Cu_2O top subcell for subsequent absorption in the c-Si bottom subcell. The ZnO/Cu_2O subcell, deposited on glass, could in this architecture serve as the module glass encapsulating the c-Si subcell, requiring insignificant changes to the design of the bottom cell. A low-absorbing polymer material such as ethylene vinyl acetate (EVA), which is a commonly used encapsulant material in commercial solar cell modules, could serve as the intermediate encapsulant layer.

The optical analysis presented in this work involves using ray tracing methods to calculate the spectral curves for reflectance, absorptance, and transmittance for different thicknesses of the thin film layers constituting the ZnO/Cu_2O subcell. Such analysis can provide guidelines for layer thickness optimization to ensure efficient light management for the STHSC device [13] [14].

2. Adopted Simulation Model

Figure 2 shows a schematic representation of the STHSC simulation model that was adopted. The device structure includes a quartz glass superstrate, an aluminum doped ZnO (AZO) n^+-type emitter layer, a Cu_2O p-type absorber layer, and a bottom AZO electrode layer placed on top of a c-Si subcell. An alternative is to use tin-doped indium oxide (ITO) as bottom transparent conductive oxide (TCO) layer. However, the optical and electrical properties of AZO closely match those of ITO, and in addition, AZO is non-toxic and less expensive compared to ITO. The backside nitrogen doped cuprous oxide (Cu_2O:N) layer (cf. Figure 1) which is a heavily doped p+ layer incorporated in order to reduce recombination losses for the ZnO/Cu_2O subcell, has been omitted in this model. The Cu_2O:N layer is typically quite thin with optical properties that are similar

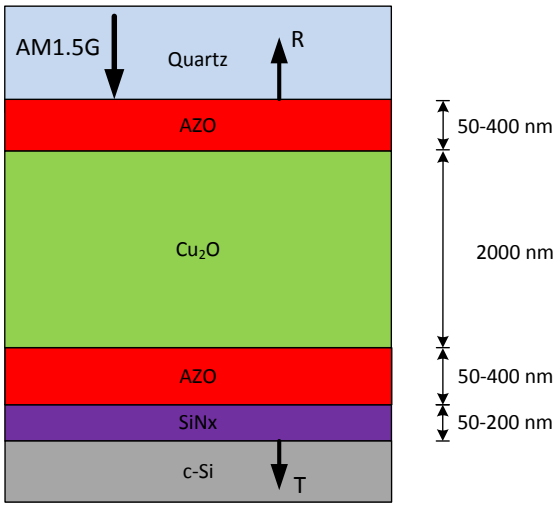

Figure 2. Schematic representation of the simulated STHSC device structure. The thickness constraints for the individual layers are indicated.

to those of Cu_2O, resulting in a minor influence on the optical characteristics of the ZnO/Cu_2O subcell.

A buffer layer can be inserted between the AZO emitter layer and the Cu_2O layer in order to reduce the band offset at the interface. Zn(O,S), (Zn,Ge)O, Ga_2O_3, and TiO_2 thin films have been employed as such buffer layers [12] [15]. In this model, the buffer layer is omitted since the thickness of the buffer layer is usually less than ~10 nm and thus will not have a major influence on the optical characteristics of the ZnO/Cu_2O subcell. Furthermore, the encapsulation layer which is intermediate between the two subcells has also been omitted in the model. Although this layer typically will have low absorption in the visible and near-infrared wavelength range, its introduction will result in increased reflection losses for the STHSC.

For evaluating the effect of the thin film layer thicknesses on the optical characteristics of the STHSC device we used OPAL 2 developed by PV Lighthouse [16]. Planar (flat) surfaces were adopted in the simulation model and the incident optical spectrum was air mass 1.5 global (AM1.5G). The reflectance (R), absorptance (A), and transmittance (T) were calculated for the wavelength range from 300 nm to 1100 nm. Here, R is the ratio of the light escaping the front quartz/AZO interface to the incident light, including reflections from all interfaces in the layered structure, A is the ratio of the light absorbed in the AZO, Cu_2O, and SiN_x layers to the incident light, and T is the ratio of the light that is transmitted into the c-Si substrate to the incident light. For the quartz glass, the crystalline silicon substrate, and the silicon nitride anti-reflection layer, tabulated values for the refractive index were adopted [17] [18] [19], whereas for the AZO and Cu_2O layers experimentally determined complex refractive indices were implemented. The thickness constraints for the AZO and Cu_2O layers are indicated in **Figure 2**. For the AZO layers, a low sheet resistance is required in order to provide sufficient lateral transport of charge carriers. Hence the lower bound for the AZO layer thickness was set to 50 nm. For the Cu_2O absorber

layer, the experimentally feasible thickness range is typically a few micrometers, due to the relative low deposition rate for the sputtered thin film. The thickness of the silicon nitride (SiN_x) anti-reflection coating for the c-Si subcell was varied in the range from 50 nm to 200 nm.

3. Experimental Techniques

Cu_2O and AZO thin films were deposited on 10 × 10 × 0.5 mm^3 quartz substrates using a direct current/radio frequency (DC/RF) magnetron sputtering system (Semicore Triaxis). The quartz substrates were cleaned in piranha and rinsed in deionized water. Subsequently, the substrates were blown dry with nitrogen and loaded into the deposition chamber. Cu_2O was deposited by reactive sputtering of a 99.999% Cu target in O_2/Ar (6/49 sccm) with a substrate temperature of 400˚C. The power density was fixed at 2.2 W/cm^2. As-grown Cu_2O films were annealed at 900˚C for 3 minutes in vacuum (pressure ~10^{-1} Torr) in order to enhance the optical and electrical properties. AZO was deposited by co-sputtering of a 99.99% pure ZnO ceramic target and a 99.999% Al target in Ar with a substrate temperature of 400˚C, yielding an aluminum content of approximately 4 wt% in the deposited layers. During the magnetron sputtering deposition, the base pressure was kept below 3.0 × 10^{-7} Torr and the sample stage was rotated at a constant speed of 12 rpm during the deposition. The optical properties and surface morphology of the AZO and Cu_2O thin films were analyzed using a Horiba Jobin Yvon UVISEL spectroscopic ellipsometer in the wavelength range from 300 nm to 800 nm at an incident angle of 70˚ and a QUANTA INSPECT F 50 scanning electron microscope (SEM), respectively. The optical transmittance spectrum in the wavelength range from 300 nm to 1000 nm was measured using a setup with spectrophotometers, a deuterium-halogen light source, and an integrating sphere. Room temperature Hall effect measurements (LakeShore 7604) using the van-der Pauw method were carried out to determine the carrier mobility, resistivity, and carrier concentration of the AZO and Cu_2O thin films.

4. Results and Discussion

4.1. Refractive Index and Surface Morphology

Figure 3(a) shows the recorded spectroscopic ellipsometry parameters Ψ and Δ for a 200 nm thick AZO thin film on quartz, along with the numerical fits to the measured curves. A Tauc-Lorentz dispersion formula was adopted for modelling of absorption in the ultra-violet wavelength range due to electronic transition, whereas a Drude dispersion formula was implemented for modelling free-carrier absorption in the near-infrared wavelength. The mean squared error (MSE) for the fit was 4.9. The extracted refractive index n and extinction coefficient k for the AZO layer are shown in **Figure 3(b)**, corresponding well with dispersions relations previously reported for AZO films [20]. Aluminum doping of ZnO results in n-type conductivity and the generated free carriers (electrons) increase the optical absorption in the near-infrared wavelength range. This can be ob-

served in Figure 3(b), which shows a slightly increasing extinction coefficient with increasing wavelength for the AZO thin film.

Figure 4 shows the recorded spectroscopic ellipsometry parameters Ψ and Δ for a 500 nm thick as-grown and annealed Cu_2O thin film on quartz, along with the numerical fits to the measured curves. The optical constants for Cu_2O were modeled using a Tauc-Lorentz dispersion formula, whereas the surface roughness was modelled by mixing the optical constants of the bulk thin film material and air. The MSE of the fit for the as-grown and annealed Cu_2O thin film was 7.9 and 10.0, respectively.

Figure 5(a) shows the calculated wavelength dispersion of the refractive index

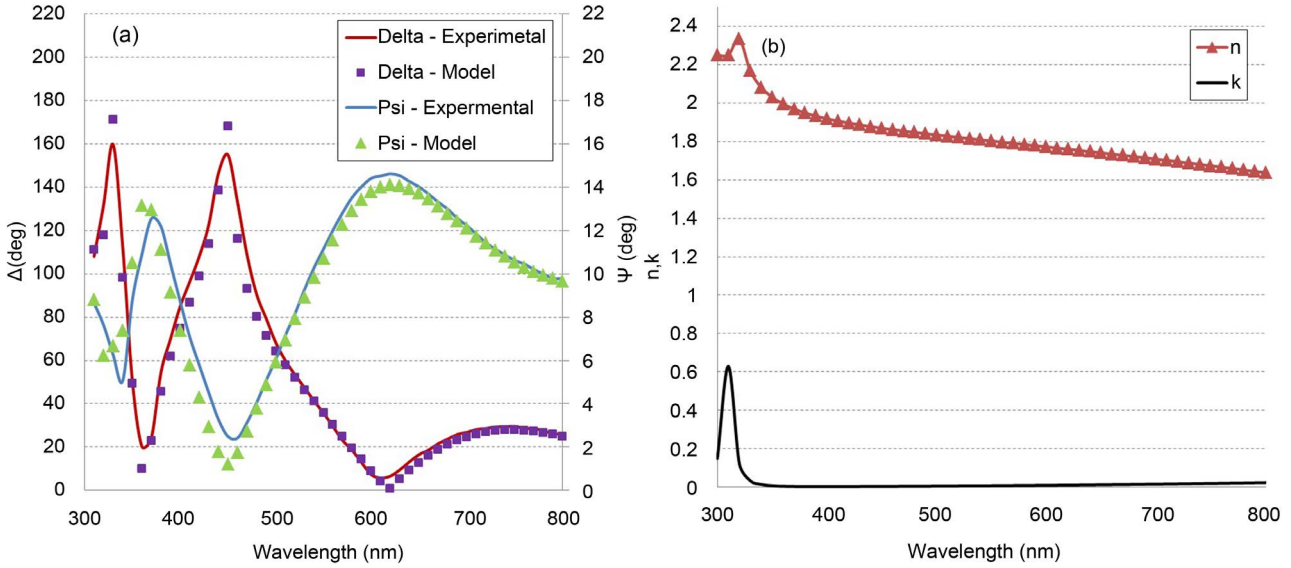

(a) (b)

Figure 3. (a) Measured spectroscopic ellipsometry data Ψ and Δ, along with numerical fits from model calculation; (b) Refractive index and extinction coefficient for a 200 nm thick AZO thin film on quartz.

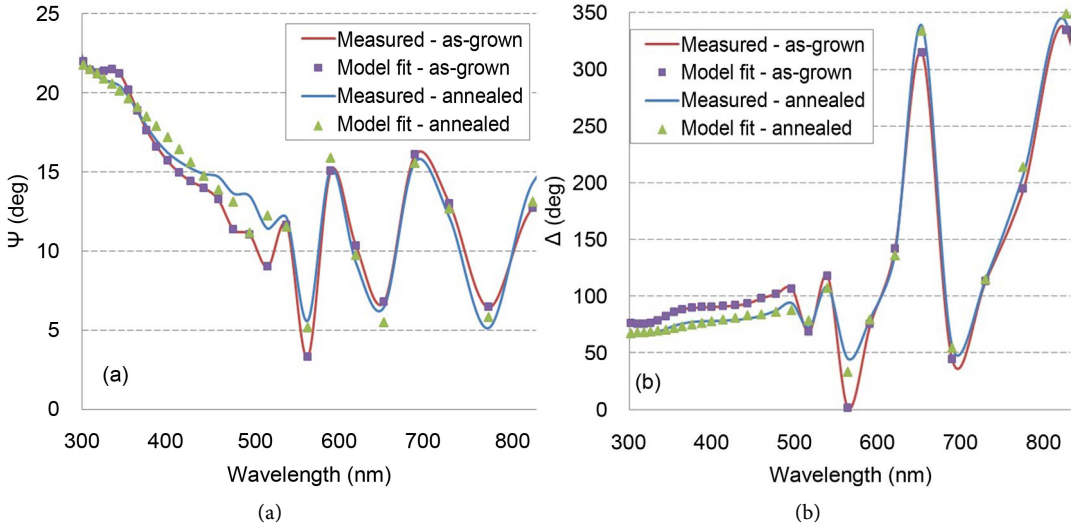

(a) (b)

Figure 4. Measured spectroscopic ellipsometry data (a) Ψ and (b) Δ for the as-grown and annealed Cu_2O thin film on quartz, along with numerical fits from model calculation.

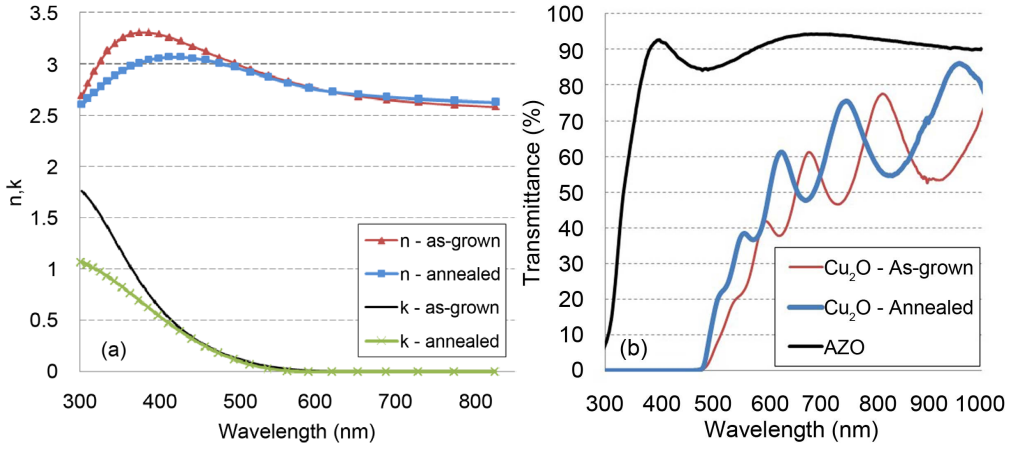

(a) (b)

Figure 5. (a) Refractive index and extinction coefficient for the as-grown and annealed Cu_2O thin film on quartz; (b) Optical transmittance spectra for the as-grown and annealed Cu_2O thin film on quartz along with AZO thin film on quartz.

n and the extinction coefficient *k* for the as-grown and annealed Cu_2O thin film, as obtained from the numerical fit to spectroscopic ellipsometry data shown in **Figure 4**. The extracted dispersion curves render a refractive index and extinction coefficient for the Cu_2O layer that correspond well with dispersion relations previously reported for Cu_2O films [21]. The curves in **Figure 5(a)** suggest that both the refractive index and extinction coefficient for the Cu_2O layer decrease in the wavelength region below ~450 nm after vacuum annealing at 900˚C. **Figure 5(b)** shows the optical transmittance spectra for a 500 nm thick as-grown and annealed Cu_2O thin film on quartz as well as a 200 nm thick AZO thin film on quartz.

Based on the measured transmittance spectra, a Tauc plot analysis was made to determine the optical band gap of the AZO and as-grown and annealed Cu_2O thin films [22]. The analysis (data not shown) suggests that the optical band gap is increased from E_g = 2.23 eV for the as-grown Cu_2O film to E_g = 2.38 eV after annealing. For the AZO thin film the optical band gap was estimated to E_g = 3.72 eV, evidencing the so-called Burstein-Moss effect.

SEM images for a 500 nm thick as-grown and annealed Cu_2O thin film on quartz are shown in **Figure 6(a)** and **Figure 6(b)**, respectively. The images show that the average grain size for the Cu_2O thin film increases from about 70 nm for the as-grown film to about 600 nm for the annealed film. The transmittance properties for the Cu_2O layer is enhanced in the visible and near-infrared wavelength range after annealing (cf. **Figure 5(b)**), which is likely due to the larger grain size and a corresponding reduction of grain-boundary scattering [23]. In general, for thin-film photovoltaic applications it is desirable to have a columnar grain structure with a lateral grain size that is larger than the thickness of the thin film [24].

Table 1 shows the values for majority carrier mobility, film resistivity, and carrier concentration for AZO and Cu_2O (as-grown and annealed) thin films on

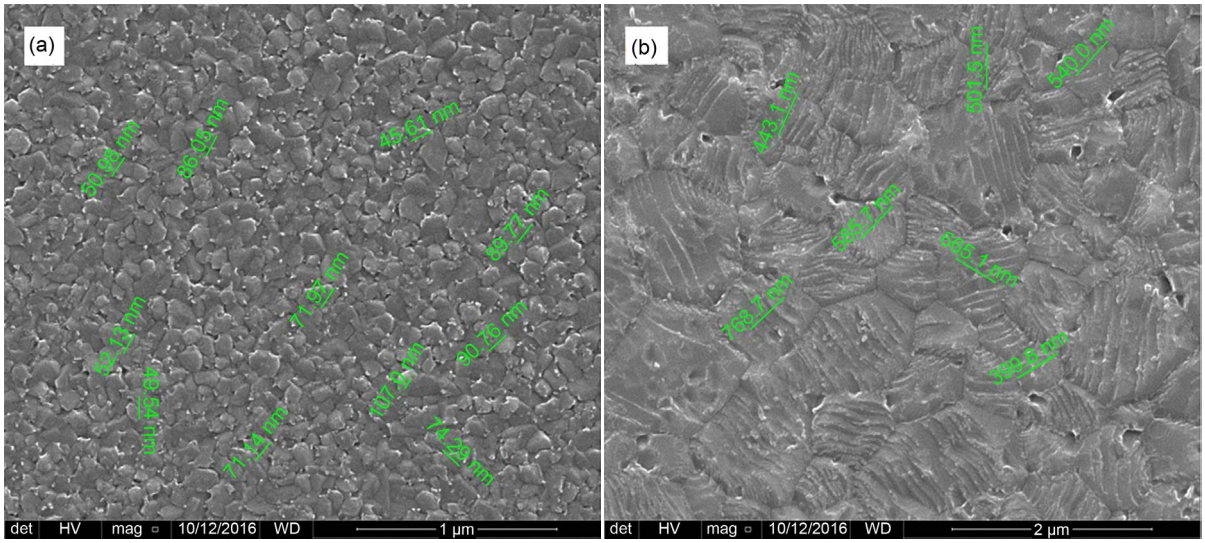

Figure 6. SEM image of (a) as-grown and (b) annealed Cu_2O thin film on quartz. The size of randomly selected grains is indicated in the images. The average grain size increases from ~70 nm for the as-grown film to ~600 nm for the annealed film.

Table 1. Carrier mobility, film resistivity, and carrier concentration for AZO and Cu_2O (as-grown and annealed) thin films on quartz, derived from room temperature hall effect measurements.

Material	Mobility [$cm^2/V{\cdot}s$]	Resistivity [$\Omega{\cdot}cm$]	Carrier concentration [cm^{-3}]
AZO	20	5×10^{-4}	3×10^{20}
Cu_2O (as-grown)	10	560	3×10^{15}
Cu_2O (annealed)	50	200	1×10^{15}

quartz. The Hall effect measurements suggest that the electrical properties for the Cu_2O thin film are enhanced after annealing, *i.e.*, the majority carrier (hole) mobility increases from 10 to 50 $cm^2/V{\cdot}s$ and the resistivity decreases from 560 to 200 $\Omega{\cdot}cm$ after annealing. These values are comparable to those reported previously for sputter-deposited polycrystalline Cu_2O thin films on quartz [25] [26], suggesting that the annealed Cu_2O thin films are well suited for photovoltaic applications. The increase in carrier mobility after annealing can, at least partly, be attributed to the increase in grain size and reduced grain-boundary scattering.

4.2. Optical Modelling

In general, thermalization losses for the STHSC device are reduced if most high energy photons are absorbed in the top subcell, and consequently, it is advantageous to absorb as much high energy photons as possible in the Cu_2O absorber layer. Figure 7(a) shows the calculated photo generated current versus thickness for the as-grown and annealed Cu_2O layer under AM1.5G illumination. The calculation shows that an annealed Cu_2O layer of 2 µm thickness will generate about 10 mA/cm^2 of photocurrent. This corresponds to about 80% of the photocurrent that can be generated for an infinitely thick layer. Figure 7(a) also shows that the photo generated current is lower for the annealed Cu_2O layer

compared to the as-grown Cu_2O layer, due to less grain-boundary scattering.

Figure 7(b) shows the calculated normalized reflectance, absorptance, and transmittance as a function of wavelength for the device model depicted in Figure 2. In this simulation, an 80 nm thick front AZO layer, a 2 μm thick Cu_2O layer, and a 75 nm thick bottom AZO layer were implemented in the model. The curves show that most of the photons with a wavelength below 600 nm are absorbed in the top ZnO/Cu_2O subcell. It can also be seen that in the long-wavelength range the AZO layers contribute to parasitic absorption, caused by free carrier absorption.

In addition to serving as a transparent conductive oxide, the top AZO emitter layer also acts as an anti-reflection layer. Thus its thickness should ideally be chosen to minimize the front reflectance and maximize the long-wavelength transmittance. Figure 8(a) shows the average percentage reflectance, absorptance,

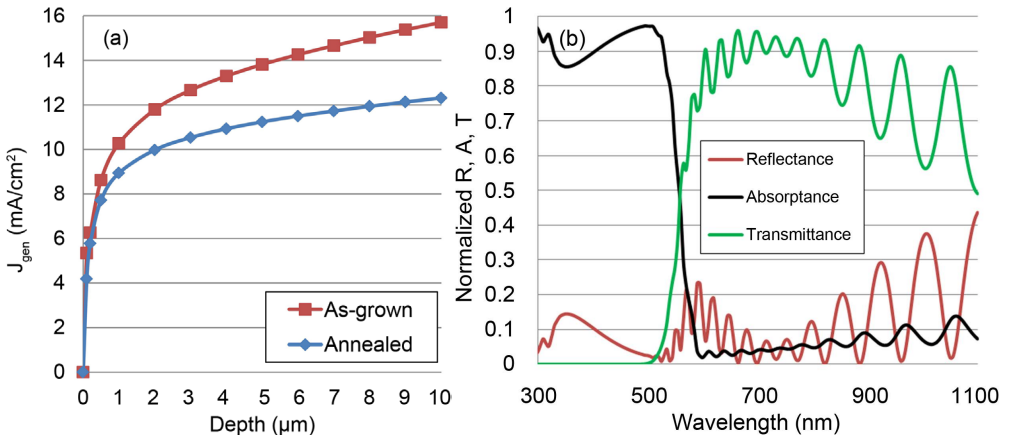

(a) (b)

Figure 7. (a) Calculated photogenerated current as a function of depth for the as-grown and annealed Cu_2O thin film under AM1.5G illumination; (b) Normalized reflectance (R), absorptance (A), and transmittance (T) as a function of wavelength for the STHSC structure.

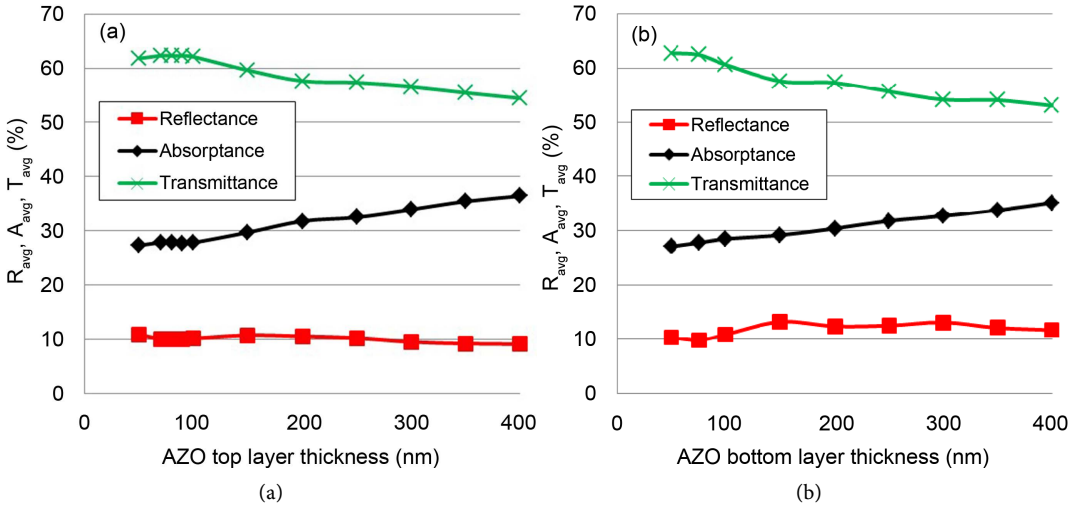

(a) (b)

Figure 8. Average percentage reflectance (R_{avg}), absorptance (A_{avg}), and transmittance (T_{avg}) for the ZnO/Cu_2O subcell as a function of thickness for the (a) top and (b) bottom AZO layer.

and transmittace as a function of thickness for the top AZO layer. In this simulation, the thickness of the Cu_2O layer was 2 μm and the thickness of the bottom AZO layer was fixed at 75 nm. The data shows that a thickness of around 80 nm for the top AZO layer results in high transmittance combined with low reflectance. Increasing the thickness of the top AZO layer beyond 100 nm results in a reduced transmittance due to the enhanced absorption in the AZO layer in the long-wavelength range ($\lambda > 550$ nm).

The average percentage reflectance, absorptance, and transmittance as a function of thickness for the bottom AZO layer are shown in **Figure 8(b)**. In this simulation, the thickness of the Cu_2O layer was 2 μm and the thickness of the top AZO layer was 80 nm. The lowest reflectance and highest transmittance are obtained for a thickness of 75 nm for the bottom AZO layer. The thickness of both the top and bottom AZO layer should ideally be kept low in order to avoid parasitic losses in the long-wavelength range. However, the thickness of the AZO transparent electrode also needs to be optimized with respect to the electrical performance of the solar cell, and typically, a thickness of about 200 nm for the AZO layer has been adopted for Cu_2O-based heterojunction solar cells [12]. **Figure 8** suggests that the average transmittance is reduced by about 5% when the thickness of the top or bottom AZO layer is increased from 80 nm to 200 nm.

The typical thickness of a SiN_x anti-reflection coating for a conventional c-Si solar cell is approximately 80 nm. However, in a STHSC device the energy spectrum of photons impinging on the c-Si bottom subcell is different compared to the conventional case since most short-wavelength photons are absorbed in the top subcell. **Figure 9(a)** shows the transmitted and absorbed spectral intensity for the ZnO/Cu_2O subcell. In order for the SiN_x layer to act as an effective anti-reflection coating, its thickness should be increased from the standard thickness

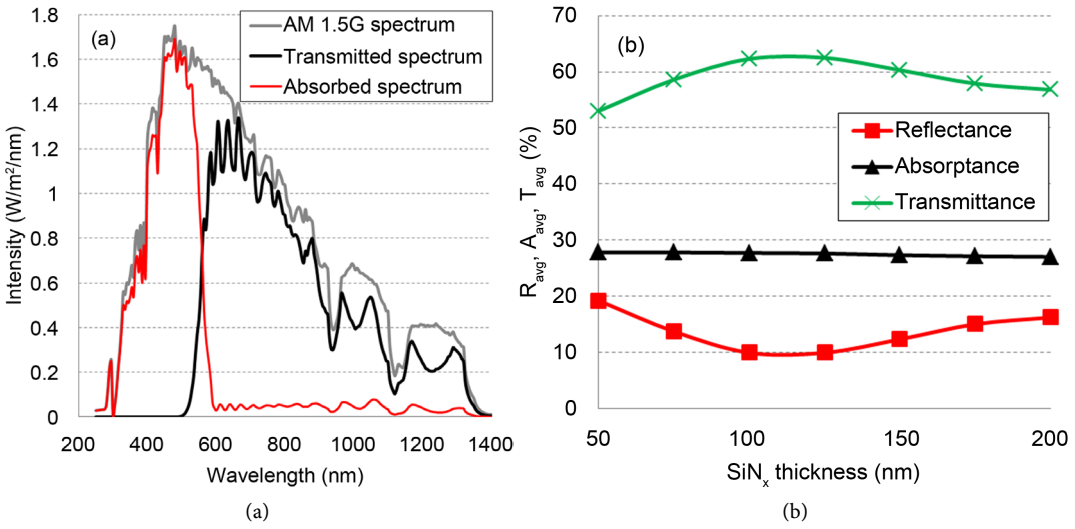

Figure 9. (a) Absorbed and transmitted spectral intensity for the ZnO/Cu_2O subcell along with the AM1.5G spectrum; (b) Average percentage reflectance (R_{avg}), absorptance (A_{avg}), and transmittance (T_{avg}) for the ZnO/Cu_2O subcell as a function of thickness for the SiN_x layer.

to accommodate the shift of the photon spectrum towards longer wavelengths. The average percentage reflectance, absorptance, and transmittance as a function of thickness for the SiN_x layer are shown in **Figure 9(b)**. The calculations show that the lowest reflectance and highest transmittance are obtained for a thickness of approximately 120 nm for the SiN_x layer. By increasing the thickness of the SiN_x layer from 80 nm to 120 nm, the total reflectance for the STHSC device is reduced from 12.7% to 9.7%.

5. Conclusions

The optical analysis presented in this work focused on calculating the spectral curves for reflectance, absorptance, and transmittance for different thicknesses of the thin film layers constituting the ZnO/Cu_2O subcell of a silicon-based tandem heterojunction solar cell. Characterization of the sputter-deposited Cu_2O thin films showed that annealing at 900˚C enhances the electrical properties and reduces optical absorption, presumably as a result of increased grain size. Hall effect measurements showed that the majority carrier (hole) mobility increased from 10 to 50 $cm^2/V{\cdot}s$ and the resistivity decreased from 560 to 200 Ω·cm after annealing. For a 2 μm thick Cu_2O absorber layer about 10 mA/cm^2 of photocurrent will be available for collection current under AM1.5G illumination, corresponding to about 80% of the photocurrent that can be generated for an ifinitely thick layer. The lowest reflectance and highest transmittance for the ZnO/Cu_2O subcell were obtained for a thickness of approximately 80 nm for both the top and bottom AZO layers. In a tandem configuration, the optical properties of the SiN_x anti-reflection coating for the c-Si bottom subcell must be optimized to accommodate the shift of the photon spectrum towards longer wavelengths.

In conclusion, the sputter-deposited Cu_2O thin films presented in this work show good potential for application as an absorber layer in a silicon-based tandem heterojunction solar cell. So far, an architecture consisting of planar (non-textured) layers has been analyzed by optical modelling, providing guidelines for layer thickness optimization to ensure efficient light management. The impact of light trapping schemes on the optical performance, as well as modelling of the electrical characteristics of the silicon-based tandem heterojunction solar cell, will be the subject of further investigation.

Acknowledgements

This work was conducted under the research project “High-performance tandem heterojunction solar cells for specific applications (SOLHET)”, financially supported by the Research Council of Norway (RCN) and the Romanian Executive Agency for Higher Education, Research, Development and Innovation Funding (UEFISCDI) through the M-Era.net program.

References

[1] White, T.P., Lal, N.N. and Catchpole, K.R. (2014) Tandem Solar Cells Based on High Efficiency C-Si Bottom Cells: Top Cell Requirements for >30% Efficiency,

IEEE Journal of Photovoltaics, **4**, 208-214.
https://doi.org/10.1109/JPHOTOV.2013.2283342

[2] Futscher, M.H. and Ehrler, B. (2016) Efficiency Limit of Perovskite/Si Tandem Solar Cells. *ACS Energy Letters*, **1**, 863-868. https://doi.org/10.1021/acsenergylett.6b00405

[3] Dmiroth, F. (2016) 30.2 Percent Efficiency—New Record for Silicon-Based Multi-Junction Solar Cell. Fraunhofer-Institut für Solare Energiesysteme ISE, Press Release.

[4] Diao, S., Zhang, X., Shao, Z., Ding, K., Jie, J. and Zhang, X. (2017) 12.35% Efficient Graphene Quantum Dots/Silicon Heterojunction Solar Cells Using Graphene Transparent Electrode. *Nano Energy*, **31**, 359-366.
https://doi.org/10.1016/j.nanoen.2016.11.051

[5] Zhang, D., Soppe, W. and Schropp, R.E. (2015) Design of 4-Terminal Solar Modules Combining Thin-Film Wide-Bandgap Top Cells and C-Si Bottom Cells. *Energy Procedia*, **77**, 500-507. https://doi.org/10.1016/j.egypro.2015.07.071

[6] Baranwal, A.K., Shiki, T., Ogomi, Y., Pandey, S.S., Ma, T. and Hayase, S. (2014) Tandem Dye-Sensitized Solar Cells with a Back-Contact Bottom Electrode without a Transparent Conductive Layer. *RSC Advances*, **4**, 47735-47742.
https://doi.org/10.1039/C4RA07539K

[7] Liu, M., Johnston, M.B. and Snaith, H.J. (2013) Efficient Planar Heterojunction Perovskite Solar Cells by Vapour Deposition. *Nature*, **501**, 395-398.
https://doi.org/10.1038/nature12509

[8] Zhanga, D., Verheesa, W., Dörenkämpera, M., Qiub, W., Bakkera, K., Gutjahra, A., Veenstraa, S., Gehlhaarb, R., Ulrich, R., Paetzold, W., Soppea, W., Romijna, I., Geerligsa, L.J., Aernoutsb T. and Weebera, A. (2016) Combination of Advanced Optical Modelling with Electrical Simulation for Performance Evaluation of Practical 4-Terminal Perovskite/C-Si Tandem Modules. *Energy Procedia*, **92**, 669-677.
https://doi.org/10.1016/j.egypro.2016.07.039

[9] Fara, L. and Yamaguchi, M. (2013) Advanced Solar Cell Materials, Technology, Modeling, and Simulation. IGI Global Publishing House, Hershey.
https://doi.org/10.4018/978-1-4666-1927-2

[10] Svensson, B.G., Pearton, S.J. and Jagadish, C. (2013) Oxide Semiconductors, Semiconductors and Semimetals. Vol. 88, Elsevier & Academic Press, Amsterdam.

[11] Shockley, W. and Queisser, H.J. (1961) Detailed Balance Limit of Efficiency of PN Junction Solar Cells. *Journal of Applied Physics*, **32**, 510-519.
https://doi.org/10.1063/1.1736034

[12] Minami, T., Nishi, Y. and Miyata, T. (2016) Efficiency Enhancement Using a $Zn_{1-x}Ge_x$-O Thin Film as an N-Type Window Layer in Cu_2O-Based Heterojunction Solar Cells. *Applied Physics Express*, **9**, Article ID: 052301.
https://doi.org/10.7567/apex.9.052301

[13] Filipič, M., Löper, P., Niesen, B., De Wolf, S., Krč, J., Ballif, C. and Topič, M. (2015) CH3NH3PbI3 Perovskite/Silicon Tandem Solar Cells: Characterization Based Optical Simulations. *Optics Express*, **23**, 263-278.
https://doi.org/10.1364/OE.23.00A263

[14] Albrecht, S., Saliba, M., Correa-Baena, J.-P., Jäger, K., Korte, L., Hagfeldt, A., Grätzel, M. and Rech, B. (2016) Towards Optical Optimization of Planar Monolithic Perovskite/Silicon-Heterojunction Tandem Solar Cells. *Journal of Optics*, **18**, Article ID: 064012. https://doi.org/10.1088/2040-8978/18/6/064012

[15] Brandt, R.E., Young, M., Park, H.H., Dameron, A., Chua, D., Lee, Y.S., Teeter, G., Gordon, R.G. and Buonassisi, T. (2014) Band Offsets of N-Type Electron-Selective

Contacts on Cuprous Oxide (Cu_2O) for Photovoltaics. *Applied Physics Letters*, **105**, Article ID: 263901. https://doi.org/10.1063/1.4905180

[16] Baker-Finch, S.C. and McIntosh, K.R. (2012) OPAL 2: Rapid Optical Simulation of Silicon Solar Cells. *Proceedings of the* 38t*h IEEE Photovoltaic Specialists Conference*, Austin, 3-8 June 2012, 265-271.

[17] Malitson, I.H. (1965) Interspecimen Comparison of the Refractive Index of Fused Silica. *Journal of the Optical Society of America*, **55**, 1205-1208. https://doi.org/10.1364/JOSA.55.001205

[18] Green, M. and Keevers, M. (1995) Optical Properties of Intrinsic Silicon at 300 K. *Progress in Photovoltaics*: *Research and Applications*, **3**, 189-192. https://doi.org/10.1002/pip.4670030303

[19] Duttagupta, S., Ma, F., Hoex, B., Mueller, T. and Aberle, A. (2012) Optimised Anti-reflection Coatings Using Silicon Nitride on Textured Silicon Surfaces Based on Measurements and Multidimensional Modeling. *Energy Procedia*, **15**, 78-83. https://doi.org/10.1016/j.egypro.2012.02.009

[20] Li, Q.H., Zhu, D., Liu, W., Liu, Y. and Ma, X.C. (2008) Optical Properties of Al-Doped ZnO Thin Films by Ellipsometry. *Applied Surface Science*, **254**, 2922-2926. https://doi.org/10.1016/j.apsusc.2007.09.104

[21] Malerba, C., Biccari, F., Ricardo, C.L.A., D'Incau, M., Scardi P. and Mittiga, A. (2011) Absorption Coefficient of Bulk and Thin Film Cu_2O. *Solar Energy Materials and Solar Cells*, **95**, 2848-2854. https://doi.org/10.1016/j.solmat.2011.05.047

[22] Gan, J., Venkatachalapathy, V., Svensson, B.G. and Monakhov, E.V. (2015) Influence of Target Power on Properties of Cu_xO Thin Films Prepared by Reactive Radio Frequency Magnetron Sputtering. *Thin Solid Films*, **594**, 250-255. https://doi.org/10.1016/j.tsf.2015.05.029

[23] Wang, Y., Miska, P., Pilloud, D., Horwat, D., Mücklich, F. and Pierson, J.F. (2014) Tranmittance Enhancement and Optical Band Gap Widening of Cu_2O Thin Films after Air Annealing. *Journal of Applied Physics*, **115**, Article ID: 073505.

[24] Imaizumi, M., Ito, T., Yamaguchi, M. and Kaneko, K. (1997) Effect of Grain Size and Dislocation Density on the Performance of Thin Film Polycrystalline Silicon Solar Cells. *Journal of Applied Physics*, **81**, 7635-7640. https://doi.org/10.1063/1.365341

[25] Lee, Y.S., Winkler, M.T., Siah, S.C., Brandt, R. and Buonassisi, T. (2011) Hall Mobility of Cuprous Oxide Thin Films Deposited by Reactive Direct-Current Magnetron Sputtering. *Applied Physics Letters*, **98**, Article ID: 192115. https://doi.org/10.1063/1.3589810

[26] Ishizuka, S., Maruyama, T. and Akimoto, K. (2000) Thin-Film Deposition of Cu_2O by Reactive Radio-Frequency Magnetron Sputtering. *Japanese Journal of Applied Physics*, **39**, L786-L788. https://doi.org/10.1143/jjap.39.l786